Repositorio Institucional de la Universidad Autónoma de Madrid

https://repositorio.uam.es

Esta es la **versión de autor** del artículo publicado en:
This is an **author produced version** of a paper published in:

Advanced Materials 29.15 (2017): 1605267

DOI: http://doi.org/10.1002/adma.201605267

Copyright: © 2017 Wiley-VCH

El acceso a la versión del editor puede requerir la suscripción del recurso
Access to the published version may require subscription

OI: 10.1002/((please add manuscript number))
Article type: Communication

Title: **Two-dimensional arrays of hexagonal plasmonic necklaces for enhanced SHG**

*Alejandro Gómez-Tornero, Christos Tserkezis, Luis Mateos, Luisa E. Bausá and Mariola O Ramírez**

A. Gómez-Tornero, Prof. L. E. Bausá, Dr. M. O Ramírez
Departamento Física de Materiales and Instituto Nicolás Cabrera
Universidad Autónoma de Madrid,
Madrid 28049, Spain
E-mail: mariola.ramirez@uam.es

Dr. C. Tserkezis
Department of Photonics Engineering
Technical University of Denmark
Kgs. Lyngby, 2800, Denmark

Dr. L. Mateos
Optoelectronics Research Centre,
University of Southampton,
Southampton SO17 1BJ, United Kingdom.

Keywords: ((ferroelectrics, silver nanoparticles, plasmonic necklaces, second harmonic generation))

Advanced nonlinear light sources capable to operate in extremely confined volumes (sub-wavelength scale) are of significant relevance in a number of applications including label free molecular sensing, integrated photon sources for quantum communication, (bio)-imaging or photocatalysis.[1-5] On the other hand, nonlinear dielectric media are extensively used in macroscopic devices to produce frequency conversion processes, and constitute the basis of numerous monolithic light sources currently exploited in quantum optics, photonics or ultrafast spectroscopies.[6,7] Several approaches, including, for instance, metamaterials based on non-centrosymmetric stacks of nanolaminates, [8] have been used to incorporate nonlinear materials on novel photonic platforms. However, at nanometric dimensions the reduced interaction length between the fundamental and the generated harmonic waves drastically

reduces the nonlinear conversion efficiency. This limitation can be overcome by exploiting the unique ability of plasmonic nanostructures to enhance and confine the electromagnetic fields of light in sub-wavelength scales by means of the excitation of localized surface plasmon resonances (LSP).[9] Most of the current strategies for second harmonic generation (SHG) at the nanoscale are focused on the intrinsic nonlinearity of the metallic nanostructures themselves. In particular, an intense activity is nowadays devoted to the fabrication and characterization of different designs of metallic nanostructures with non-centrosymmetric geometries. [10-15]

A different approach to exploit the local electric field enhancement and boost the SHG response at sub-wavelength scales is based on the association of nonlinear dielectrics with metallic nanostructures supporting LSPs able to strongly confine and enhance the electric fields involved in the nonlinear process. In these plasmonic/nonlinear-dielectric hybrid systems, the metallic nanostructures act as efficient nano-antennas enhancing the interactions between the incident far-field light and the SHG by the nonlinear substrate in the vicinity of the metallic nanostructures. [16-18] However, despite its potential, the association of nonlinear dielectric materials with plasmonic nanostructures is still hindered by the technological challenge of precisely placing the nonlinear material in the vicinity of plasmonic hot-spots, thus constraining further development of hybrid plasmonic/nonlinear dielectric systems.

In this work we use hexagonal ferroelectric domain walls as artificial 2D sub-micrometer patterns on which strongly interacting Ag nanoparticles (NPs) can be formed in the shape of hexagonal necklaces. Specifically, we combine ferroelectric domain engineering and polarization-mediated chemistry to obtain finely designed two-dimensional (2D) plasmonic arrays of hexagonal supercells distributed on the polar surface of a $LiNbO_3$ crystal. The hexagonal plasmonic necklaces support broad radiative plasmonic resonances allowing a further enhancement of SHG at the ferroelectric domain boundaries, which act as nanometric

nonlinear sources. In particular, we show that, through this cost-effective engineering approach, a 400-fold SHG enhancement can be achieved at the near UV spectral region. The work opens the way for the easy, cost-efficient design of complex geometries of plasmonic NPs, thus facilitating further design of waveguides, splitters and corners with enhanced nonlinear response of interest for nanoscale optical devices.

To build up the hybrid plasmonic/nonlinear-dielectric system, we used a spatially-selective surfactant-free process based on the photo-reduction of metallic cations on the polar surface of a ferroelectric domain structure.[19] This simple procedure (usually referred to as ferroelectric lithography) has been successfully employed for the formation of different noble metal nanostructures on ferroelectric domain surfaces. Direct growth of nanowires or linear chains of metallic nanoparticles on the surfaces of domain boundaries, or silver nanocubes on ferroelectric domain surfaces have been recently reported.[20-22] However, the potential of this method to produce functional plasmonic nanostructures into organized 2D metasurfaces has not been addressed yet. The organization of strongly interacting closely spaced metallic NPs into 2D supercells is of large interest to explore and promote a broad range of light-matter interaction processes at the nanoscale such as phase control, polarization switching or nonlinear devices with extended functionalities.[23,24] Our approach experimentally validates the feasibility of assembling large areas of designed 2D plasmonic arrays on top of functional ferroelectrics and exploits the nonlinearity of the host to produce SHG process at the nanoscale with enhancement values exceeding two orders of magnitude. Because of the flexibility of the fabrication procedure and the remarkable improvement of the nonlinear response at the nanoscale, this work represents a step towards the development of efficient frequency converter nano-devices by means of a scalable and simple production. Moreover, in ferroelectric crystals, the extension of the domain patterns from 1D (PPLN structures) to a 2D geometry would allow the access to multi-directional and multi-wavelength frequency

conversion phenomena. Namely, Cerenkov type SHG or nonlinear Raman Nath diffraction have been demonstrated in 2D nonlinear crystals, [25-27] offering a very different spatial distribution and polarization of the radiated waves with respect to the 1D case - for instance, multicolor radially polarized high-harmonic rings has been reported in $LiNbO_3$.[27] Thus, merging the potentiality of 2D domain patterns for nonlinear interactions with 2D plasmonic arrays would allow the enhancement and manipulation of radiated waves with very different characteristics from those of a 1D case. This feature would expand the development of advanced nonlinear sources with reliable multifunctional optical character for the next generation of optical devices.

Prior to the metallic deposition, 2D ferroelectric domain patterns were fabricated in areas of 0.4 x 0.4 mm^2 by using direct electron beam writing (DEBW) as a tool to reverse the spontaneous polarization of the $LiNbO_3$ substrate. Compared to conventional poling techniques based on electrical electrodes, the use of DEBW enables patterning of ferroelectric domain structures with large versatility and without any masking process.[28,29] In our case, the fabricated 2D templates consisted of square lattices of hexagonal domains of different sizes and separations. After the ferroelectric patterning, the ferroelectric substrate was immersed into an $AgNO_3$ solution and illuminated with above bandgap UV radiation (λ= 254 nm). This allowed the formation of chains of Ag NPs on the domain boundaries surfaces without the need of any additional chemical reactive or surfactant (See methods).[19,30] **Figure 1** shows SEM images of the polar surface after the selective deposition of Ag NPs on the hexagonal domain walls surfaces. Hexagonal necklaces are formed by nearly spherical Ag NPs of around 50 nm in size with average interspacing distances of about 2 nm (Figure 1a), which ensure strong field interaction among them. To illustrate the scalability of the process, the SEM images in panels b-d show arrangements of the plasmonic necklaces with different sizes and separation distances ranging from 1 to 10 μm. The schematic of the fabrication steps is depicted in Figure 1e.

Figure 2 shows the optical response of the plasmonic necklaces. The dark field microscopy images of two different 2D patterns are shown in Figure 2a. As seen, for hexagon sizes from 1–10 μm, the scattering response displays a dominant orange-yellowish colour, which does not depend on the necklace size as discussed below. Additionally, in contrast to the marked polarization character displayed by linear arrangements of Ag NPs,[31,32] the far-field spectral response of the plasmonic modes sustained by the necklaces remains invariant regardless of the polarization direction. The corresponding experimental extinction spectrum, obtained in transmission mode, is displayed in Figure 2b. It exhibits a broad resonance extending from the near UV down to the near infrared spectral region, useful for NIR to VIS frequency conversion processes.

To obtain further physical insight into the plasmonic response of the hexagonal unit cells, we have performed numerical simulations for perfect regular hexagons containing different number of Ag NPs, *i.e* hexagonal necklaces with different side lengths. To better understand the nature of the modes, we started with the smallest possible hexagon, consisting of just 6 NPs (so that each hexagon side contains two NPs), and gradually increase the size of the cell. Figure 2c shows the calculated extinction spectrum for a hexagon containing 54 NPs (10 NPs per side). As seen, it consists of two main bands. The one located in the near UV spectral region (325-390 nm) is governed by the plasmon resonance sustained by individual particles. The band located in the low energy region (λ >400 nm) corresponds to the collective excitation of the NPs forming the necklace. This large mode broadens and shifts to longer wavelengths as we increase the necklace size, until it eventually saturates at around 530 nm for hexagons containing ~10 NPs per side (54 NPs) (Figure S1 in the Supporting Information). Such optical response is in agreement with that reported for chains of NPs in linear arrangements in which, for the same size of NPs (~50 nm), an effective length of about 10-15 NPs was found to be adequate for the collective mode to saturate (stop red shifting).[33,34] In

fact, the simulations show that the optical response of the hexagonal necklace can be efficiently analyzed by the embedded chain plasmon model,[33,35] the complex structure being decomposed into simpler linear or quasi-linear NP chains. That is, following a hopping-like mechanism, the plasmon mode propagates along the hexagon from particle to particle, as long as the external field polarization allows the efficient excitation of each subsequent NP dimmer. The optical response of the hexagons is therefore dominated by this broad, long-wavelength plasmonic chain mode which, as reported for long linear chains, is characterized by a strong radiative nature.[36] The comparison between the calculated extinction spectrum and the experimentally measured one obtained after subtracting the contribution from the bare $LiNbO_3$ substrate is displayed in Figure 2 c. As it can be seen, the spectral features are in very good agreement.

Once the plasmonic modes supported by the necklaces were examined, the nonlinear response from the hybrid plasmonic/$LiNbO_3$ structures was studied by analyzing the spatially resolved SHG in confocal geometry. The fundamental wavelength was tuned from 780 to 860 nm. Two bandpass filters were used to block the fundamental and other unwanted light. **Figure 3a** shows the spatial map obtained by integrating the SHG radiation at 390 nm when the fundamental beam was tuned at 780 nm. The selected spatial region comprises eight plasmonic necklaces with diameters of about 2 μm. As clearly observed, the SHG is mainly obtained when the fundamental beam is focused on the proximity of the metallic arrangements. Indeed, the nonlinear signal replicates the 2D distribution of the plasmonic necklaces revealing a substantial enhancement of the SHG response relative to the bare substrate. Similar results were obtained for necklaces with different sizes. To better illustrate this aspect, Figure 3b shows a detail of the SHG image of a single large motif (diameter ~10 μm) together with the SHG intensity as a function of the spatial position across the diameter of the plasmonic necklace. In fact, the SHG intensity from the bare substrate is negligible

compared to that obtained from the domain boundary surfaces where the Ag NPs are located. These results are consistent with the nanoscale confinement and field enhancement driven by the plasmonic modes sustained by the necklaces. To estimate the enhancement factor we conducted a set of scans on the same substrate in the absence of metallic nanostructures. In this case, the incident pump power had to be increased an order of magnitude (~ 10 mW) to achieve a measurable signal. A SHG intensity profile is included in Figure 3b for the sake of comparison (red dots). As seen, in the absence of Ag NPs, the nonlinear response generated at the domain boundaries is between 2 and 3 times that of the surface in agreement with the local symmetry changes of the ferroelectric domain wall surface.[37,38] Under these experimental conditions the SHG intensity from the bare substrate can be compared to that obtained at the immediacy of the metallic arrangements when excited with a pump power of 1mW. Therefore, according to the quadratic dependence of the SHG signal on the fundamental radiation, it can be concluded that the nonlinear response generated at the domain walls is enhanced by more than two orders of magnitude due to the plasmonic necklaces. Table SI in the supplementary section summarizes the SHG results obtained for the three cases of interest, *i.e* single domain region far away from domain walls (LNB), ferroelectric domain walls in the absence of metallic nanostructures (LNB +DW) and domain wall surfaces on which strongly coupled Ag nanoparticles were deposited (LNB+DW+NPs).

A point that should be addressed concerns frequency conversion processes spatially localized at domain walls in ferroelectrics. It is well established that symmetry breaking at the domain boundaries strongly affects the condition for SHG at those regions.[39-44] Indeed, the change in the local symmetry at domain walls can results into a brighter signal of the SHG response upon certain configurations.[40,42-44] On the other hand, destructive interference between the SHG signal from opposite domains can also lead to a (partial) cancelation of the monitored SHG.[39] Figure S2 in the Supporting Information details the behavior of the bare domain wall surfaces for different polarization configurations. In our experimental conditions

the fundamental laser beam was carefully focused on the crystal surface in order to diminish the SHG contribution arising from opposite domains.

To analyze the role of the electric field polarization state on the measured SHG in the vicinities of the metallic nanostructures, the generated nonlinear response was analyzed for different input/output polarization configurations of the fundamental and SHG beams (**Figure 4**a). We first compare the effect of orthogonal polarizations of the fundamental beam on the generated nonlinear response (top panels in Fig. 4a). As seen, the spatial distribution of the SHG intensity exhibits a noticeable polarization dependence on the incident radiation. More specifically, the SHG intensity reaches maximum values for a fundamental beam with electric field components parallel to the NPs alignments and decreases when the electric field is perpendicular to them. This polarization dependence is opposite to that obtained in the absence of metallic nanostructures (Figure S2 in the Supporting Information), and confirms the coupling of the plasmonic modes supported by the metallic necklaces with the incident electric field involved in the frequency conversion process. The bottom panels in Figure 4a show the simulated near field distribution at the long-wavelength plasmon resonance for the same two polarizations. Although the spectral properties of the plasmonic necklaces are polarization-independent, as we verified by detailed simulations. This near-field distribution is dramatically affected by the incident polarization, in agreement with recent works.[45] Note that for every polarization, the fundamental beam excites chain modes with different orientations along the hexagon. Thus, for the long-wavelength plasmonic mode (λ>400nm), the electric field enhancement significantly decreases when the side of the hexagon is excited by an incident beam polarized perpendicular to it. The calculations agree well with the experimental results and point out the capability of SHG as a nanometric tool to probe the local plasmonic fields in hybrid nonlinear platforms. On the other hand, rotating the polarization of the SHG output signal at 380 nm affects the spatial SHG intensity distribution to a much lesser extent than the fundamental radiation. Let us recall that, according to

previous reports, the long-wavelength band observed in the extinction spectrum shows a dominant radiative character, whereas, absorption is dominant in the high energy region (λ~325-390 nm).[36] Therefore, the observed increase in the SHG mainly arises from the enhancement of the fundamental radiation driven by plasmonic coupling. To deeper highlight this aspect we studied the spectral dependence of the experimental enhancement factor as a function of the fundamental wavelength (Figure 4b). The enhancement values were determined by comparing the measured SHG from the hybrid metal/nonlinear dielectric system with that obtained from the surface of the bare substrate. As observed, in the analyzed spectral region, the enhancement values are significantly increased when the fundamental beam is tuned to the long-wavelength plasmonic resonance. In fact, average enhancement values up to 400 are obtained when the fundamental beam is varied from 840 nm to 780 nm (SHG at 420 and 390 nm, respectively). That is, even though the extinction values sustained by the necklaces are similar at 420 nm and 780 nm (Figure 2c), the participation of two near-infrared photons of the fundamental beam makes the enhancement of the fundamental radiation the dominant mechanism of the SHG intensification. Therefore, the spectral and polarization behavior of the enhanced SHG is consistent with the quadratic pump power dependence of SHG on the fundamental beam and can be accounted for in terms of the plasmonic response of the metallic necklaces. In this sense, the polarization independent spectral response supported by the necklaces provides a crucial advantage for spectrally matching the interacting waves involved in the nonlinear process and allows for a broad tunability of the SHG response. On the other hand, the possibility of controlling the spatial location of the plasmonic hot spots by optical fields along with the sensitivity of SHG introduces new avenues for sensing and light control in all optical nano-devices.[46]

In summary, we have experimentally validated the ability of ferroelectric lithography for the directed formation of 2D arrays of plasmonic necklaces in large-scale spatial regions by using functional ferroelectric templates in $LiNbO_3$. The association of metallic nanostructures

supporting strongly coupled plasmonic modes with the nonlinear material has been exploited for enhanced nonlinear optics at the nanoscale. We demonstrate an enhancement of the SHG response of two orders of magnitude compared to the case of the bare crystal. This value is among the highest intensification values reported for a hybrid plasmonic/nonlinear system. Furthermore, the larger enhancement values are obtained for SHG in the near UV range, with the subsequent potential technological impact. The cost-effective and versatile approach for fabricating scalable plasmonic super-structures could be extended to other type of ferroelectric systems such as molecular ferroelectric crystals [47] or multiferroic metal-organic frameworks,[48] with attributes useful for molecular or flexible optoelectronics. The results herein may open up alternative avenues to obtain hybrid plasmonic metamaterials with applications in a diversity of areas including high-density data storage, optical circuits, quantum optical systems or ultra-sensitive detection.

Experimental Section

Sample preparation

Commercial Z-cut congruent $LiNbO_3$ crystals were irradiated by directly focusing the e-beam provided by a Philips XL30 Schottky field emission gun electron microscope on the Z^- face of the crystal. An Elphy Raith nanolithography software was employed to design the 2D pattern. The total written areas were as large as 0.4x0.4 mm^2. During the electron irradiation, the Z^+ face of the crystal was coated with a 100 nm film of Al which acted as a ground electrode. The acceleration voltage and the beam current were fixed at 15kV and 0.3 nA, respectively. The applied charge density was varied between 600 and 3000 $\mu C/cm^2$ depending on the desired domain size and lattice periods. The inverted domains were directed along the ***c*** polar axis of the crystal and crossed the whole thickness of the sample (around 0.5 mm).[29]

The photo-induced silver deposition process was carried out on optically grade polished crystals by illuminating during 4 minutes the polar surface of the patterned ferroelectric crystal with above band gap UV light (Mercury pen-lamp UVP model 11SC-1) while the crystal was immersed in a 0.01M $AgNO_3$ solution at 60 ºC. Details on the procedure can be found elsewhere.[19,21,30] For the analysis of the average nanoparticle size and interspacing distances, nanometric-scaled images with magnifications of up to 200000x were obtained by a scanning electron microscope (SEM) model Philips XL30 SFEG.

Optical characterization

Dark field microscopy images were obtained in transmission configuration by using an Olympus BX51 microscope equipped with a dark-field condenser. The extinction measurements were obtained with a UV/vis/NIR Lambda 1050 PerkinElmer spectrometer. The spectra were measured in transmission configuration using a spot size of 5 mm^2. The contribution of the plasmonic necklaces to the extinction spectrum was obtained after subtracting the signal from bare (non-plasmonic) $LiNbO_3$ substrate.

Spatially resolved SHG experiments were performed on a customized scanning confocal microscope (Olympus BX41) provided with a two-axis XY motorized platform (0.2 μm spatial resolution) driven by Labspec software. A tunable femtosecond Ti:sapphire laser (Spectra Physics Model 177-Series), used as a fundamental beam, was focused onto the sample surface by using a 100x microscope objective. The SHG signal was collected in backscattering geometry with the same objective and detected by a Peltier cooled photomultiplier tube. The fundamental wavelength was tuned from 780 to 860 nm and the incident power was kept below 1 mW to avoid damaging the plasmonic structures.

Numerical calculations

Numerical calculations were performed using the Multiple Multipole Method,[49] which is efficient for the analysis of large NP clusters.[33,34] Each spherical NP was modelled by a multipole of order 3 placed at the center of the sphere. Additional multipoles were placed close to the gaps to capture the strong NP interaction. In all cases, we simulated regular hexagons of 50-nm Ag Nps separated by 2-nm gaps, in air, illuminated by a plane wave polarized along one of the hexagon sides (x-axis).

Supporting Information

Supporting Information is available from the Wiley Online Library or from the author.

Acknowledgements

This work has been supported by the Spanish Ministry of Economy and Competitiveness (MINECO) under projects MAT2013-43301-R and MAT2016-76106-R and Comunidad de Madrid under grant S2013/MIT-2740. CT was supported by funding from the People Programme (Marie Curie Actions) of the European Union's Seventh Framework Programme (FP7/2007-2013) under REA grant agreement number 609405 (COFUNDPostdocDTU).

Received: ((will be filled in by the editorial staff))
Revised: ((will be filled in by the editorial staff))
Published online: ((will be filled in by the editorial staff))

References

[1] M. Kauranen, A. V. Zayats, *Nat. Photonics* **2012**, *6*, 737.

[2] J. D. Cox, I. Silveiro, F. J. García de Abajo, *ACS Nano* **2016**, *10*, 1995.

[3] A.V. Kachynski, A. Pliss, A. N. Kuzmin, T. Y. Ohulchanskyy, A. Baev, J. Qu, P. N. Prasad, *Nat. Photonics* **2014**, *8*, 455.

[4] C. Clavero, *Nat. Photonics* **2014**, *8*, 95.

[5] P. Pantazis, J. Maloney, D. Wu, S. E. Fraser, *Proc. Natl. Acad. Sci. U.S.A.* **2010**, *107*, 14535.

[6] H. Y. Leng, X. Q. Yu, Y. X. Gong, P. Xu, Z. D. Xie, H. Jin, C. Zhang, S. N. Zhu, *Nat. Communications* **2011**, *2*, 429.

[7] V. Ramaiah-Badarla, A. Esteban-Martin, M. Ebrahim-Zadeh, *Laser Photonics Rev.* **2013**, *7*, 55.

[8] L. Alloatti, C. Kieninger, A. Froelich, M. Lauermann, T. Frenzel, K. Köhnle, W. Freude, J. Leuthold, M. Wegener, C. Koos, *Appl. Phys. Lett*. **2015**, *107*, 121903.

[9] S. F. Maier, *Plasmonics: Fundamentals and applications*, Springer, New York, USA **2007**.

[10] M. Celebrano, X. Wu, M. Baselli, S. Großmann, P. Biagioni, A. Locatelli, C. De Angelis, G. Cerullo, R. Osellame, B. Hecht, L. Duò, F. Ciccacci, M. Finazzi, *Nat. Nanotechnol*. **2015**, *10*, 412.

[11] R. Czaplicki, J. Mäkitalo, R. Siikanen, H. Husu, J. Lehtolahti, M. Kuittinen, M. Kauranen, *Nano Lett.* **2015**, *15*, 530.

[12] J. Butet, P. F. Brevet, O. J. F. Martin, *ACS Nano* **2015**, *9*, 10545.

[13] Z. Dong, M. Asbahi, J. Lin, D. Zhu, Y. M. Wang, K. Hippalgaonkar, H. S. Chu, W. P. Goh, F. Wang, Z. Huang, J. K. W. Yang, *Nano Lett.* **2015**, *15*, 5976.

[14] B. Metzger, L. Gui, J. Fuchs, D. Floess, M. Hentschel, H. Giessen, *Nano Lett.* **2015**, *15*, 3917.

[15] M. B. Raschke, S. Berweger, J. M. Atkin, *Ultrafast and Nonlinear Plasmon Dynamics*, Springer, New York, USA, 237, **2014.**

[16] H. Linnenbank, Y. Grynko, J. Förstner, S. Linden, *Light: Sci. Appl.* **2016**, *5*, 16013.

[17] D. Lehr, J. Reinhold, I. Thiele, H. Hartung, K. Dietrich, C. Menzel, T. Pertsch, E. B. Kley, A. Tünnermann, *Nano Lett.* **2015**, *15*, 1025.

[18] L. Sánchez-García, C. Tserkezis, M. O Ramírez, P. Molina, J. J. Carvajal, M. Aguiló, F. Díaz, J. Aizpurua, L. E. Bausá, *Opt. Express* **2016**, *24*, 8491.

[19] S. V. Kalinin, D. A. Bonnell, T. Alvarez, X. Lei, Z. Hu, R. Shao, J. H. Ferris, *Adv. Mater.* **2004**, *16*, 795.

[20] A. Haussmann, P. Milde, C. Erler, L. M. Eng, *Nano Lett.* **2009**, *9*, 763.

[21] E. Yraola, P. Molina, J. L. Plaza, M. O Ramírez, L. E. Bausá, *Adv. Mater.* **2013**, *25*, 910.

[22] L. Sánchez-García, M. O Ramírez, P. Molina, F. Gallego-Gómez, L. Mateos, J. J. Carvajal, M. Aguiló, F. Díaz, C. de las Heras, L. E. Bausá, *Adv. Mater.* **2014**, *26*, 6447.

[23] J. Li , S. Chen, H. Yang, J. Li, P. Yu, H. Cheng, C. Gu, H.-T. Chen, J. Tian, *Adv. Funct. Mater.* **2015**, *25*, 704.

[24] S. Keren-Zur, O. Avayu, L. Michaeli, T. Ellenbogen, *ACS Photonics* **2016,** *3*, 117.

[25] V. Berger, *Phys. Rev. Lett.* **1998**, *81***,** 4136

[26] Y. Sheng, W. Wang, R. Shiloh, V. Roppo, A. Arie, W. Krolikowski *Opt. Lett.* **2011**, *36*, 3266.

[27] L. Mateos, P. Molina, J. Galisteo, C. López, L. E. Bausá, M. O. Ramírez, *Opt. Express* **2012**, *20*, 29940.

[28] A. C. G. Nutt, V. Gopalan, M. C. Gupta, *Appl. Phys. Lett*. **1992**, *60*, 2828.

[29] L. Mateos, L. E. Bausá, M. O. Ramírez, *Appl. Phys. Lett*. **2013**, *102*, 042910.

[30] (a) Y. Sun , B. S. Eller , R. J. Nemanich , *J. Appl. Phys.* **2011** , *110*, 084303. (b) Y. Sun, R. J. Nemanich , *J. Appl. Phys*. **2011** , *109*, 104302

[31] B. Willingham, S. Link, *Opt. Express* **2011**, *19*, 6450.

[32] E. Yraola, L. Sánchez-García, C. Tserkezis, P. Molina, M. O Ramírez, J. Aizpurua, L. E. Bausá. *J. Lumin.* **2016**, *169*, 569.

[33] R. Esteban, R. W. Taylor, J. J. Baumberg, J. Aizpurua, *Langmuir* **2012**, *28*, 8881.

[34] C. Tserkezis, R. W. Taylor, J. Beitner, R. Esteban, J. J. Baumberg, J. Aizpurua, *Part. Part. Syst. Charact.* **2014**, *31*, 152.

[35] R. W. Taylor, R. Esteban, S. Mahajan, J. Aizpurua, J. J. Baumberg, *J. Phys. Chem. C* **2016**, *120*, 10512.

[36] E. Yraola, L. Sánchez-García, C. Tserkezis, P. Molina, M. O Ramírez, J. L. Plaza, J. Aizpurua, L. E. Bausá, *Opt. Express* **2015**, *23*, 15670.

[37] E. A. Eliseev, A. N. Morozovska, S. V. Kalinin, Y. Li, J. Shen, M. D. Glinchuk, L.-Q. Chen, V. Gopalan, *J. Appl. Phys.* **2009**, *106*, 084102.

[38] V. R. Aravind, A. N. Morozovska, S. Bhattacharyya, D. Lee, S. Jesse, I. Grinberg, Y. L. Li, S. Choudhury, P. Wu, K. Seal, A. M. Rappe, *Phys. Rev. B* **2010**, 82, 024111.

[39] S. A. Denev, T. T. A. Lummen, E. Barnes, A. Kumar, V. Gopalan, *J. Am. Ceram. Soc.* **2011**, *94*, 2699.

[40] M. Flörsheimer, R. Paschotta, U. Kubitscheck, Ch. Brillert, D.Hofmann, L. Heuer, G. Schreiber, C. Verbeek, W. Sohler, H. Fuchs, *Appl. Phys. B* **1998**, 67, 593.

[41] A. Vasudevarao, A. Kumar, L. Tian, J. H. Haeni, Y. L. Li, C.-J. Eklund, Q. X. Jia, R. Uecker, P. Reiche, K. M. Rabe, L. Q. Chen, *Phys. Rev. Lett.* **2006**, 97, 257602.

[42] S. I. Bozhevolnyi, J. M. Hvam, K. Pedersen, F. Laurell, H. Karlsson, T. Skettrup, M. Belmonte, *Appl. Phys. Lett.* **1998**, *73*, 1814.

[43] A. Fragemann, V. Pasiskevicius, F. Laurell, *Appl. Phys. Lett*. **2004**, *85*, 375.

[44] S. I. Bozhevolnyi, K. Pedersen, T. Skettrup, X- Zhang, M. Belmonte, *Opt. Comm.* **1998**, *152*, 221.

[45] R. Thomas, R. S. Swathi, *J. Phys. Chem. C* **2016**, *120*, 18733.

[46] V. Kravtsov, R. Ulbricht, J. M. Atkin, M. B. Raschke. Nat. nanotechnol. **2016**, *11*, 459.

[47] D.W. Fu, H.L. Cai, Y. Liu, Q. Ye, W. Zhang, Y. Zhang, X.Y. Chen, G. Giovannetti, M. Capone, J. Li, R.G. Xiong, *Science* **2013,** *339*, 425.

[48] D.W. Fu, W. Zhang, H.L. Cai, Y. Zhang, J.Z Ge, R. G. Xiong, S. D. Huang, T. Nakamura *Angew. Chem. Int. Ed.*, **2011**, *50*, 11947.

[49] T. Sannomiya, J. Vörös, C. Hafner, *J. Comput. Theor. Nanosci.* **2009**, *6*, 749.

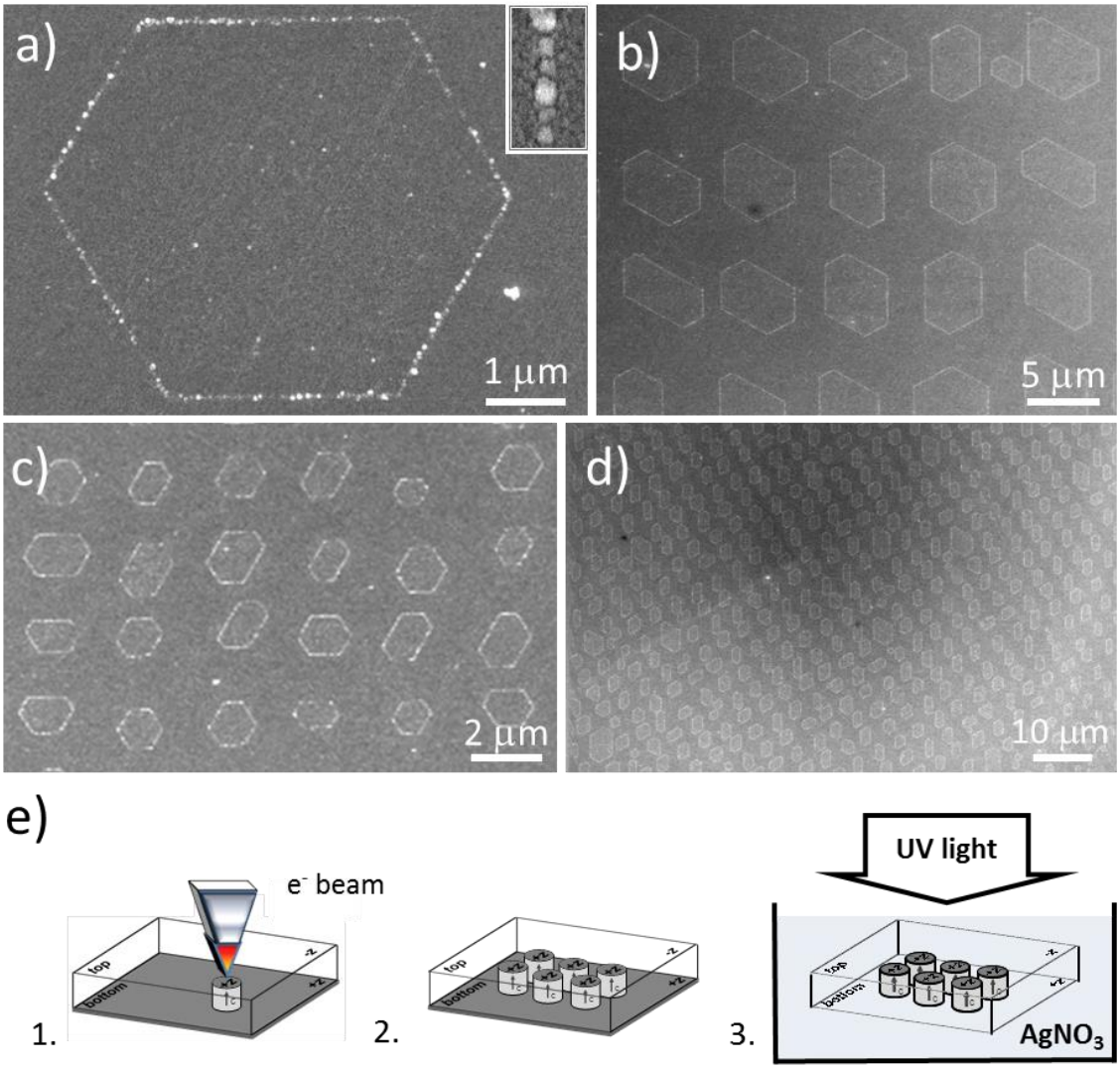

Figure 1. 2D plasmonic necklaces ordered in large-scale spatial regions by using functional ferroelectric templates in $LiNbO_3$**.** (a-d) SEM images of the selectively formed Ag NPs necklaces on the hexagonal domain boundary surfaces in $LiNbO_3$ after the photochemical procedure. The plasmonic necklaces are ordered in a 2D geometry (square lattice) and were fabricated on the same substrate. To illustrate the scalability of the process as well as the possibility to obtain different sizes and geometries, SEM images obtained with different magnifications are shown. The inset in panel (a) shows a detailed view of the NPs forming the necklace. Their average size is 50 nm with interspacing distances of about 2 nm. (e) Schematics of the fabrication steps: 1-2. Fabrication of 2D ferroelectric domain pattern by electron beam writing. 3. Photo-induced silver deposition process by UV irradiation. The crystal is immersed in $AgNO_3$.

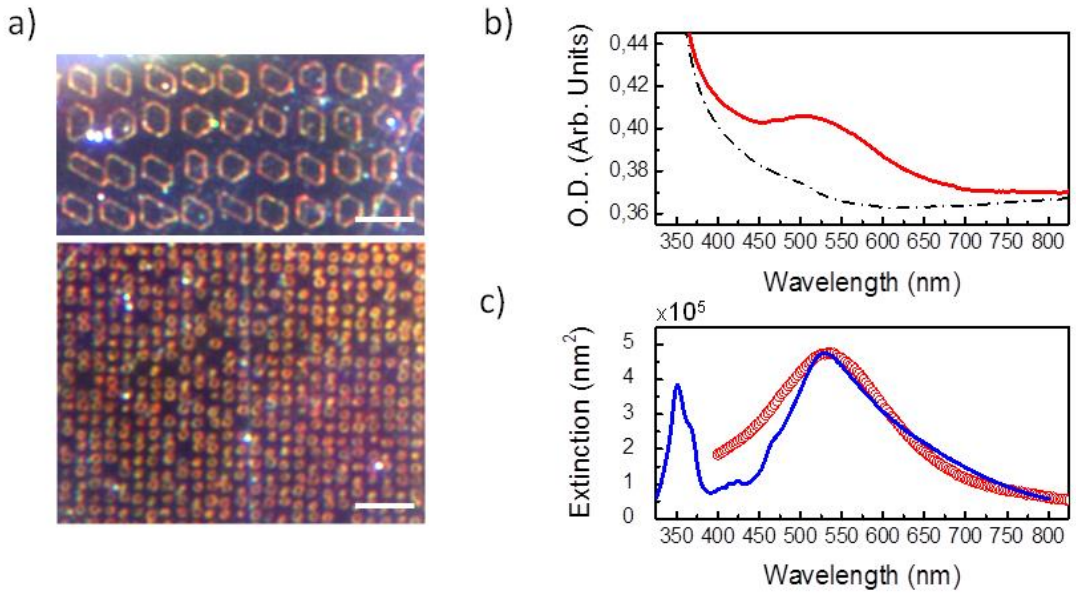

Figure 2. Optical response of the plasmonic necklaces. (a) Examples of dark field microscopy images showing the visible light scattered from two different patterns consisted of hexagonal plasmonic necklaces with the same NP sizes (50 nm) assembled on $LiNbO_3$ substrate. The scale bar in both panels is 10 μm. (b) Extinction spectrum from bare $LiNbO_3$ crystal (black dashed line) and from the hybrid plasmonic system (red line). (c) Experimental extinction spectrum obtained in transmission mode after subtracting the contribution from the bare $LiNbO_3$ substrate (red dots); Theoretical extinction spectra supported by metallic necklaces of 54 NPs (blue line). For the sake of comparison the experimental spectrum has been normalized to the maximum intensity of the theoretical one.

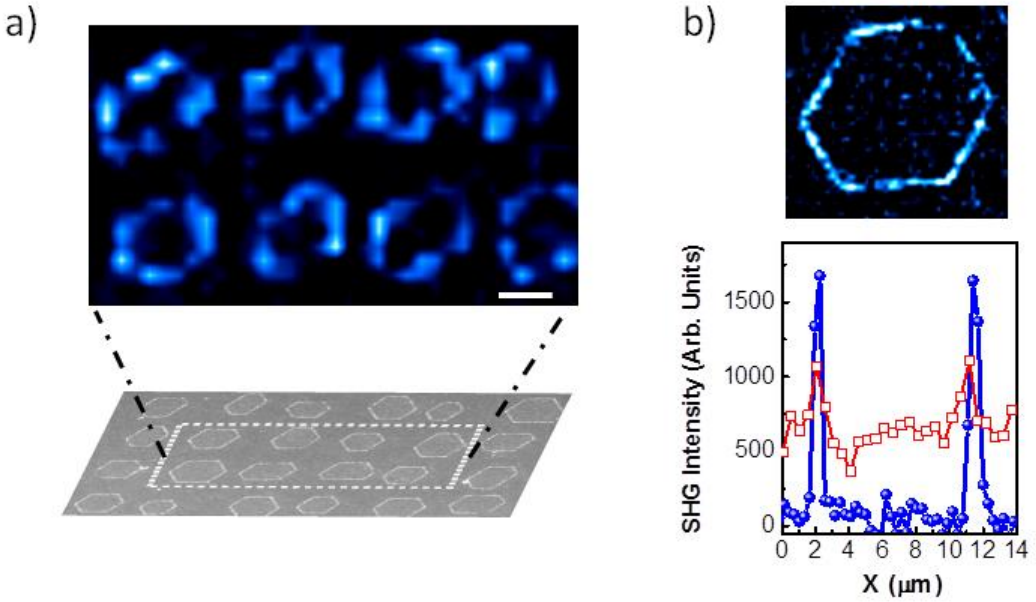

Figure 3. Spatially resolved SHG image from the hybrid plasmonic-$\chi^{(2)}$ nonlinear system. (a) SHG spatial map of a selected spatial region comprising eight hexagons with diameters of 2 μm separated by a distance of about 1 μm. The blue regions in the map correspond to the highest SHG intensity. The fundamental wavelength was tuned at 780 nm. The scale bar is 2μm (b) Top panel: SHG image of a single hexagonal plasmonic necklace with a length side of about 7 μm (diameter close to 10 μm). Bottom panel: Comparison of the SHG intensity profiles obtained from two samples with and without silver nanoparticles deposited on the domain walls (blue and red, respectively). Due to the strong enhancement provided by the Ag NPs on the domain wall surfaces and to make possible the comparison, the incident pump power had to be increased by an order of magnitude when the bare system was analyzed (red dots).

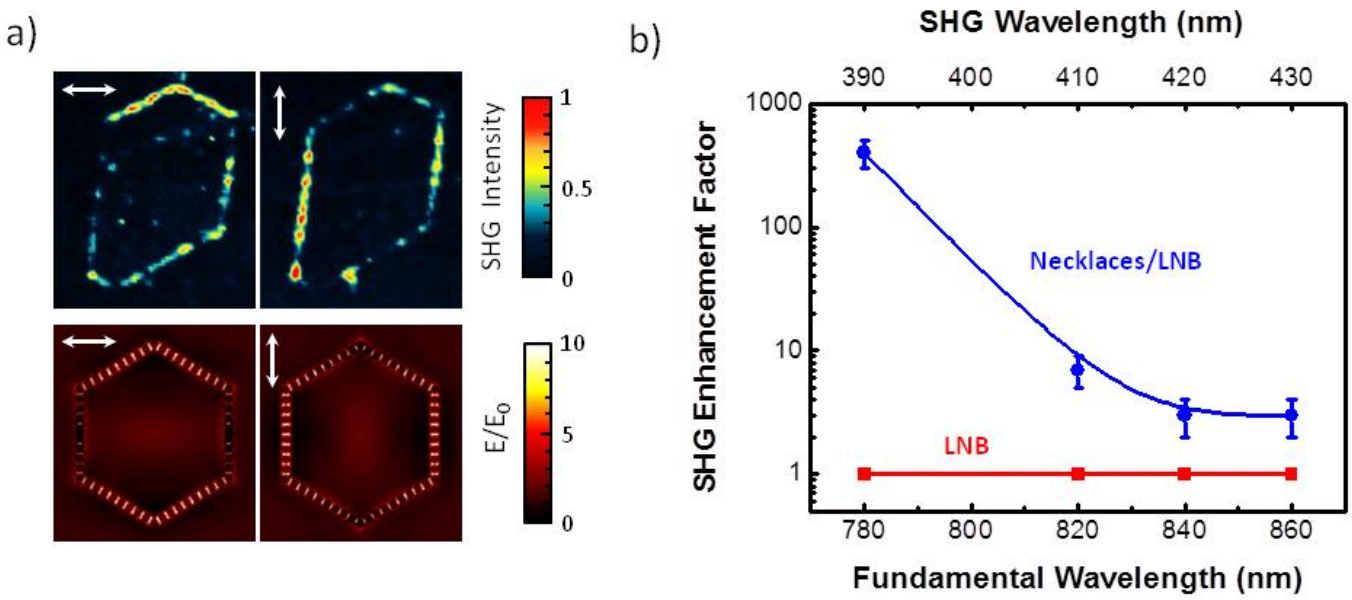

Figure 4. Polarization dependence of the plasmon enhanced SHG. (a) Top panels: Spatial distribution of the SHG intensity obtained for orthogonal polarizations of the fundamental beam. Bottom panels: Calculated near-field intensity distribution associated with the long wavelength plasmon mode excited with orthogonal polarizations. The polarization state is indicated by arrows. (b) Spectral dependence of the experimentally obtained SHG enhancement factor as a function of the fundamental wavelength.